Microstructural Investigation of High-Volume Fly Ash Composites Containing Nano-Calcium Silicate Hydrate Crystals

Zhiyuan Zhou[1]; Massoud Sofi[2]; Ylias Sabri[3]; Junli Liu[4]; Shaobo Kang[5]; and Priyan Mendis[6]

Abstract: This paper reports on the effect of addition of nano-calcium silicate hydrate (nano-CSH) seeds on the early-age strength development and microstructural evolution of concrete containing high-volume fly ash (HVFA). Cement replacement levels of 60% and 70% are considered. For each of the replacement levels, 0.5%, 1%, and 1.5% of the mass of fly ash (FA) are replaced with nano-CSH crystals. The early-age compressive strength of concrete was tested at the ages of 1, 3, 7, 14, and 28 days. Microstructural investigations involve thermogravimetric analysis (TGA), Fourier-transform infrared spectroscopy (FTIR), and scanning electron microscopy (SEM). The results show that addition of 1% and 1.5% nano-CSH seeds in HVFA60% and HVFA70%, respectively, can effectively facilitate the formation of hydration products $Ca(OH)_2$ and C-S-H as well as increase the rate of reaction and early-age strength gain at early ages. It was found that the dosages of nano-CSH seeds is a critical parameter in achieving the desired properties. **DOI: 10.1061/(ASCE)MT.1943-5533.0003974.**

Author keywords: High-volume fly ash (HVFA) composites; Nano-CSH seeds; Microstructural investigations.

Introduction

Concrete is widely produced and used as construction material because of its low cost and desirable strength. The major binder of conventional concrete is ordinary portland cement (OPC). Nevertheless, the production of cement has always raised public concerns of sustainability because nearly 1 ton of carbon dioxide is released to the atmosphere when 1 ton of OPC is produced (Malhotra and Mehta 2002). One practical way to promote the sustainability of concrete is to partially replace OPC constituents with supplementary cementitious materials (SCMs), one of which is fly ash (FA). The aim of making traditional concrete more environmentally friendly has led researches to put more emphasis on high-volume fly ash (HVFA) based concrete, in which more than 50% of OPC constituents is substituted by FA (Siddique 2004). Research shows that it is feasible to achieve a 60% or higher replacement of cement by FA to make concrete more sustainable (Huang et al. 2013; Shaikh and Supit 2014; Wongkeo et al. 2014; Gong et al. 2019; Hemalatha and Sasmal 2019). Although the addition of fly ash has positive effects on the sustainability and workability of concrete, the early-stage strength of concrete is normally negatively affected due to the prolonged setting time and extended dormant period (Sofi et al. 2012; Zhang and Islam 2012; Kocak and Nas 2014; Soutsos et al. 2016). Early-age strength is required for early load transfer and managing timely completion of the projects (Sofi et al. 2008).

With the advancement of nano-technology, nano-modification of cement-based materials has attracted great attention from the research fields. The reason why nano-material is expected to be used in the cementitious materials, including those with cement replaced by FA, is mainly because of the filler and seeding effects of nano-particles. The nano-particles speed up the hydration rate, thus improving the early-age strength of cementitious materials (Kawashima et al. 2013). Among the types of nano-particles investigated, the most widely studied material is nano-silica (Zhang and Islam 2012; Zhang et al. 2012; Shaikh et al. 2014; Jalal et al. 2015; Shaikh and Supit 2015; Supit and Shaikh 2015; Zhu et al. 2015; Shaikh et al. 2017; Liu et al. 2019; Sun et al. 2019), followed by other categories including nano-particles of zinc dioxide (ZnO) (Nazari and Riahi 2011; Yang et al. 2015; Niewiadomski et al. 2017), titanium dioxide (TiO_2) (Zhang et al. 2015; Ma et al. 2016; Niewiadomski et al. 2017; Wang et al. 2018), calcium carbonate ($CaCO_3$) (Kawashima et al. 2014; Shaikh and Supit 2014; Supit and Shaikh 2014; Shaikh and Supit 2015; Shaikh et al. 2017), and aluminum oxide (Al_2O_3) (Oltulu and Sahin 2013; Mohseni et al. 2015; Niewiadomski et al. 2017).

Studies regarding the aforementioned nano-particles have revealed that the early-age mechanical properties of cement-based materials having a portion substituted by fly ash are generally improved by different extents. For example, Sun et al. (2019)

[1]Ph.D. Candidate, Dept. of Infrastructure Engineering, Univ. of Melbourne, VIC 3010, Australia. Email: Zhiyuanz3@unimelb.edu.au

[2]Research (DECRA) Fellow, Dept. of Infrastructure Engineering, Univ. of Melbourne, VIC 3010, Australia (corresponding author). ORCID: https://orcid.org/0000-0002-0670-9278. Email: Massoud@unimelb.edu.au

[3]Research Fellow, Dept. of Infrastructure Engineering, Univ. of Melbourne, VIC 3010, Australia. ORCID: https://orcid.org/0000-0001-9422-5670. Email: ylias.sabri@rmit.edu.au

[4]Ph.D. Student, Dept. of Civil and Infrastructure Engineering, Royal Melbourne Institute of Technology, Melbourne, VIC 3001, Australia. ORCID: https://orcid.org/0000-0002-8282-8439. Email: S3847553@student.rmit.edu.au

[5]Associate Professor, School of Civil Engineering, Chongqing Univ., Chongqing 400045, China. ORCID: https://orcid.org/0000-0001-5666-6758. Email: Kang0119@cqu.edu.cn

[6]Professor, Dept. of Infrastructure Engineering, Univ. of Melbourne, VIC 3010, Australia. Email: Pamendis@unimelb.edu.au

Note. This manuscript was submitted on November 8, 2020; approved on April 13, 2021; published online on September 29, 2021. Discussion period open until February 28, 2022; separate discussions must be submitted for individual papers. This paper is part of the ***Journal of Materials in Civil Engineering***, © ASCE, ISSN 0899-1561.

evaluated the modification effects of nano-SiO_2 on early compressive strength and hydration properties of HVFA-based concrete through X-ray diffraction (XRD) and thermal gravity/differential thermal gravity (TG/DTG). The microstructural investigation results confirmed that the addition of nano-silica enhanced the formation of calcium silicate hydrate (C-S-H) gels and reduced porosity in the HVFA cement pastes, which partially compensated for the early compressive strength loss of HVFA concrete relative to OPC concrete. Similarly, Shaikh et al. (2017) studied the effects of nano-SiO_2 and nano-$CaCO_3$ on the HVFA cement pastes containing 40% and 60% Class F fly ash by microstructural investigations. They found that the addition of 2% nano-SiO_2 and 1% nano-$CaCO_3$ together into pastes contributed to the reduction of calcium hydroxide, the increase in volume fractions of C-S-H gels, and the porosity of HVFA pastes (Shaikh et al. 2017).

Research has been carried out to investigate the effect of the aforementioned nano-particles on the microstructure of HVFA concrete. Reportedly, the enhanced formation of C-S-H gels by the adding of nano-particles plays a key role in the improvement of early-age strength of HVFA concrete. Apart from the nano-particles mentioned previously, there is another type, which is nano-CSH crystal seeds. However, the studies on how the addition of nano-CSH influences the early-age strength of HVFA concrete, especially the microstructural investigations, are quite limited. Szostak and Golewski (2018) found that, by adding 4% nano-CSH into the concrete containing 20% fly ash, the strength increased over 4 times in the first 8 h. More investigations need to be done to further understand the effectiveness of using nano-CSH seeds in HVFA concrete and the underlying mechanism.

This research aims to investigate the effect of nano-CSH seeds on the compressive strength of HVFA concrete with 60% and 70% fly ash replacement at early age and up to 28 days, and to understand the underlying principles. To understand the rationale, microstructural investigation was conducted involving thermogravimetric analysis (TGA), Fourier-transform infrared spectroscopy (FTIR), and scanning electron microscopy (SEM).

Material and Experimental Work

Material and Mix Design

The cement and fly ash used in this research were supplied by Cement Australia (Darra, Queensland, Australia). Table 1 gives information about the chemical composition of cement and fly ash, and Figs. 1 and 2 illustrate the particle size distributions of cement and fly ash. The D_{V50}, the size where half of the particles reside below this point and half reside above this point in volume distribution, for fly ash and cement, is 16 μm and 18 μm, respectively. This indicates that the median size of fly ash particles is a bit smaller than, but overall similar to, that of cement particles. The fly ash is sourced from Gladstone (Cement Australia, Darra, Queensland, Australia) and is classified as Class F fly ash because the composition of fly ash satisfies $SiO_2+Al_2O_3+Fe_2O_3 \geq 70\%$ and $CaO < 10\%$ (ASTM 2005). The superplasticizer used in the experiment is MasterGlenium ACE 8710, provided by BASF Australia (Southbank, Victoria, Australia). It is polycarboxylic-based superplasticizer (SP) for retaining the workability of concrete. The recommended dosage of the MasterGlenium ACE 8710 is about 600–1200 ml per 100 kg of cementitious material (BASF 2020a). As it was found that excessive use of SP could adversely affect the compressive strength of concrete (Alaka et al. 2016), the SP added in the mix design in this research (Table 2) is within the recommended dosage range. Note in Table 2 that the dosages of SP used in the FA pastes are much lower compared with the OPC paste. This result happens because the FA particles have spherical shape, which could improve the workability of mixes (Thomas 2007), reducing

Table 1. Chemical composition of OPC and fly ash

Content		OPC	Fly ash
Chemical composition (%)	CaO	63.7	3.5
	SiO_2	19.9	55
	Al_2O_3	4.6	27.2
	Fe_2O_3	2.57	9.2
	MgO	1.39	1.21
	K_2O	0.69	0.8
	Na_2O	0.59	1.28
	P_2O_5	0.04	0.55
	Mn_2O_3	0.06	0.12
	SrO	0.07	0.05
	TiO_2	—	1.49
	SO_3	2.7	0.11
	LOI	3.9	1.2
Mineral phases (%)	C_3S	65.78	—
	C_3A	7.82	—
	C_4AF	7.88	—

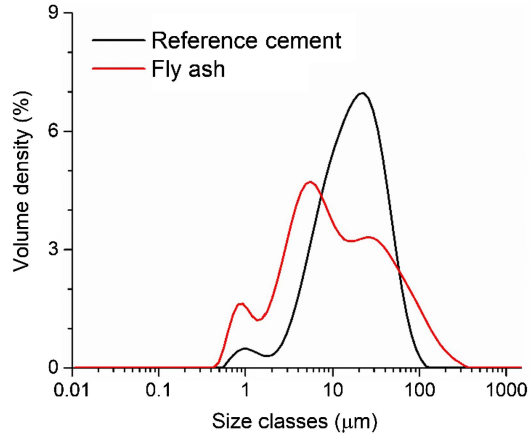

Fig. 1. Particle size distribution of materials with regard to volume density.

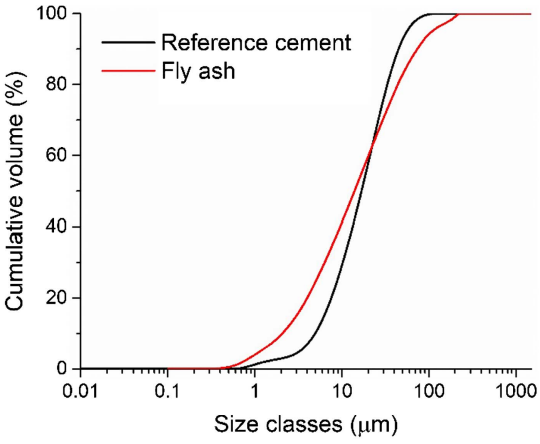

Fig. 2. Particle size distribution of materials with regard to cumulative volume.

Table 2. Mix proportion for concrete samples

Mix design		Weight per volume (kg/m^3)								
Mix	Description	Sand	7 mm aggregate	10 mm aggregate	Cement	FA	Water	SP	Master X-Seed 1500	Total
A1	FA59.5CSH0.5	628.8	15.42	1,047.68	218.25	324.65	125.42	2.64	11.86	2,374.72
A2	FA59CSH1	633.96	15.55	1,056.29	214.93	317.02	115.04	1.86	23.36	2,378.01
A3	FA58.5CSH1.5	638.98	15.67	1,064.64	211.7	309.62	104.97	1.1	34.52	2,381.19
B1	FA69.5CSH0.5	628.53	15.42	1,047.23	161.11	373.24	123.71	2.23	11.67	2,363.14
B2	FA69CSH1	633.62	15.54	1,055.71	158.7	365	113.51	1.46	23	2,366.54
B3	FA68.5CSH1.5	638.56	15.66	1,063.94	156.35	357	103.62	0.72	33.99	2,369.85
C1	FA60	623.47	15.29	1,038.8	221.68	332.52	136.13	3.45	0	2,371.34
C2	FA70	623.28	15.29	1,038.49	163.6	381.73	134.22	3.02	0	2,359.63
C3	OPC	621.97	15.25	1,036.30	611.33	0	152.83	6.348	0	2,444.03

Note: FA = fly ash; and SP = superplasticiser.

the usage of SP. The Master X-Seed 1500 (BASF Australia, Southbank, Victoria, Australia) is used in this research as the suspension of nano-CSH crystals (BASF 2020b). Master X-Seed 1500 is a type of white liquid with the suspension of 200-nm CSH nano-particles, which have the specific gravity of 1.14 ± 0.02 g/cm^3. The solid content of nano-CSH crystals is 77% in the Master X-Seed 1500 (BASF 2015). If handled or stored properly, the suspension is stable and there is no hazardous material inside. The dosages of Master-X Seed 1500 were selected to include both within and outside of the recommended range. The 0.5% nano-CSH crystals is within the recommended dosage, and the use of 1% and 1.5% nano-CSH crystals is outside of the recommended dosage.

Compression tests were conducted on all concrete samples to evaluate the effect of nano-CSH crystals on the early-age strength development. Moreover, microstructural analyses were also performed for the pastes to investigate the underlying mechanism and the physicochemical properties. These were determined using TGA, FTIR, and SEM.

The mix proportions of concrete samples are presented in Table 2 with the number behind the abbreviation of substance standing for the mass ratio of the substance in the binder. For example, FA59.5CSH0.5 represents that the FA takes up 59.5% of the binder, and the nano-CSH crystals occupies 0.5% of the binder. The mix design of pastes for microstructural investigations takes the same proportions as the corresponding concrete samples in Table 2, except that the aggregates are excluded. The calculated replacement rate of nano-CSH crystal should take into account that the nano-CSH crystal is the solid content of the Master X-Seed 1500 and occupies 77% of the total mass of the Master X-Seed 1500.

X-Ray Fluorescence

The OPC- and FA-based samples were characterized for their elemental contents using wavelength dispersive X-ray fluorescence (WD-XRF), which was conducted on a Bruker S4 pioneer X-ray spectrometer (Bruker, Karlsruhe, Germany). The samples were first calcined under air at 700°C to remove any residual organics and to ensure that all material constituents were in the oxidized form. Although such precautions were not essential for the samples used in this particular study, this standard procedure was followed to ensure the highest accuracy was achieved in the X-ray fluorescence (XRF) measurements. The XRF instruments are used to determine heavy element content within a sample and are usually inaccurate or completely blind to low molecular weight elements such as nitrogen and carbon. Therefore, it is necessary to remove organic materials within a sample to enhance the accuracy of the metal and metal oxide content measurements with this method. Calcining is mostly performed in air to make complete combustion of the organics possible, and to minimize the presence of residual carbon in the final product. Given that organic materials can degrade above 500°C (Tomczyk et al. 2020), a high calcination temperature is necessary to ensure that all organic materials are removed from the sample prior to XRF analysis (Ahmad Fara and Abdullah 2016: Xiao and Pang 2017). The samples were first calcined under air at 700°C to remove any residual organics and to ensure that all material constituents were in the oxidized form. The samples were characterized in the powder mode using He gas (over vacuum) and undergoing oxides evaluation. The samples were placed on a 6 μm Mylar pad, which is transparent in XRF measurements. Any data that did not provide material content within two decimal places and had >10% error at the same time were excluded as part of the analysis.

Thermogravimetric Analysis

The TGA was performed by using PYRIS TGA machine (PerkinElmer, Shelton, Connecticut). Prior to the commencement of TGA testing and after the pastes were cured for 28 days, the pastes were crushed and milled to transform to powder, which was required to be fine enough to pass a sieve of 63 μm. On the testing day, the hydration reaction of the pastes was stopped first, which was achieved by placing the powder of each mix on a filter paper above a vacuum pump, with the powder entirely immersed in acetone, and dried by the vacuum pump repetitively 5 times. For each mix, powder with the weight of 5–12 mg was loaded into the machine and then heated from 30°C to 1,000°C under N_2 atmosphere, with the heating rate set constantly to be 10°C/min. The TG curve plotted was based on the mass of the sample subject to heating in the percentage of original sample. The decrease in the mass of mix samples is caused by the decomposition under heating. Deboucha et al. (2017) suggested the temperature ranges for the decomposition of different compounds in the pastes, and these ranges were adopted in this research. The temperature range of 105°C–400°C mainly corresponds to the mass loss due to dehydration of C-S-H (Ldh). The range of 400°C–600°C is associated with the decomposition of $Ca(OH)_2$, called dehydroxylation (Ldx). The mass loss between 600°C and 800°C is related to the decarbonation of $CaCO_3$ (Ldc). The actual temperature ranges may be subject to minor changes with regard to the first derivative of TG curves (DTG). The calcium hydroxide (CH) content in each paste is calculated by Eq. (1) (Klimesch and Ray 1996)

$$\mathrm{CH} = 4.11\mathrm{Ldx} + 1.68\mathrm{Ldc} \tag{1}$$

The chemically bound water (W_B) is obtained using the Eq. (2), as follows (Bhatty 1986):

$$W_B = \mathrm{Ldh} + \mathrm{Ldx} + 0.41c \tag{2}$$

Fourier-Transform Infrared Spectroscopy

The FTIR test was conducted on pastes cured for 28 days. The machine used was a Perkin Elmer Spectrum 100 Fourier transform infrared spectrometer (PerkinElmer, Akron, Ohio) equipped with a universal attenuated total reflection (ATR) accessory. The procedure of controlling the software could be found in a user's guide (PerkinElmer 2005). FTIR shares the same processes as TGA in terms of preparing samples.

Scanning Electron Microscopy

The method used to observe the microstructure of pastes at 28 days was scanning electron microscopy (SEM) equipped with backscatter electron detector under the voltage of 15 V. The energy-dispersive X-ray spectroscope (EDS) was attached to the SEM apparatus to conduct elemental analysis in the pastes. Regarding the sample preparation for each mix, a small piece of paste was mounted in a cylinder mold filled with resin. The mold had a diameter of 25 mm and a height of 10 mm. The sample piece is a random fragment from the sample crushed by the compressive strength testing machine. As long as the sample is smaller than the mold, the sample could be placed into it. The surface of sample piece was polished smooth enough for the SEM test.

Results

Compressive Strength Development

Fig. 3 shows the compressive strength development of concrete with different mix designs. Observe that the compressive strengths of FA60 were 55.9% and 80.8% of OPC at 1 and 28 days, respectively. By increasing the replacement ratio of fly ash to 70%, the compressive strengths of FA70 were slightly reduced to 54.2% and 79.5% of OPC at 1 and 28 days, respectively. The slow development of HVFA concrete was mainly due to the postponed hydration of fly ash. It was found that Class F fly ash mixed in OPC could hydrate to produce CSH after about a week from the time of mixing (Neville 2011). Fly ash can participate in the chemical reaction only after the pH value in the pore solution reaches 13.2, as a result of the accumulation of $Ca(OH)_2$ generated from OPC hydration (Neville 2011). The rate of strength development of HVFA concrete was slower at an early age and accelerated at a later age, compared with OPC.

Adding nano-CSH crystals could increase the early-age compressive strength of concrete, but the extent of increase in the compressive strength depends on the dosage of nano-CSH crystals. It can be observed that for a replacement ratio of fly ash of 60%, an increase in the content of nano-CSH crystals from 0.5% to 1% increased the compressive strength, but a further increase from 1.0% to 1.5% decreased the strength at 1, 3, 7, and 28 days. The decrease of strength could be due to the reduction of cementitious material. The higher the content of nano-CSH crystals, the lower the content of cement contained in the concrete. The nano-CSH crystal itself does not have any cementitious property. It needs to interact with cement to stimulate the formation of more hydration product. Therefore, there should be an optimal dosage of nano-CSH crystals that could make concrete reach the highest strength. For the concrete with fly ash replacement ratio of 70%, adding nano-CSH crystals demonstrated a different trend in the compressive strength development. When the content of nano-CSH crystals was 0.5%, the compressive strength of FA69.5CHS0.5 was decreased as compared with FA70 without nano-CSH crystals.

The compressive strength of concrete increased with increasing content of nano-CSH crystals from 0.5% to 1.5% at 28 days. Szostak and Golewski (2018) used 4% nano-CSH crystals in OPC and concrete with 20% fly ash and also found an increase in the strength of concrete both with and without fly ash (Szostak and Golewski 2018). The mechanism could be that the nano-CSH crystals stimulated the hydration of OPC to produce more hydration products involving CSH and $Ca(OH)_2$. The formation of more $Ca(OH)_2$ could further facilitate the hydration of fly ash to generate C-S-H. Because C-S-H was the compound responsible for the majority of concrete properties, including compressive strength (Nonat 2010), the strength of concrete was increased due to the formation of CSH. This conclusion will be further verified in the microstructural investigation.

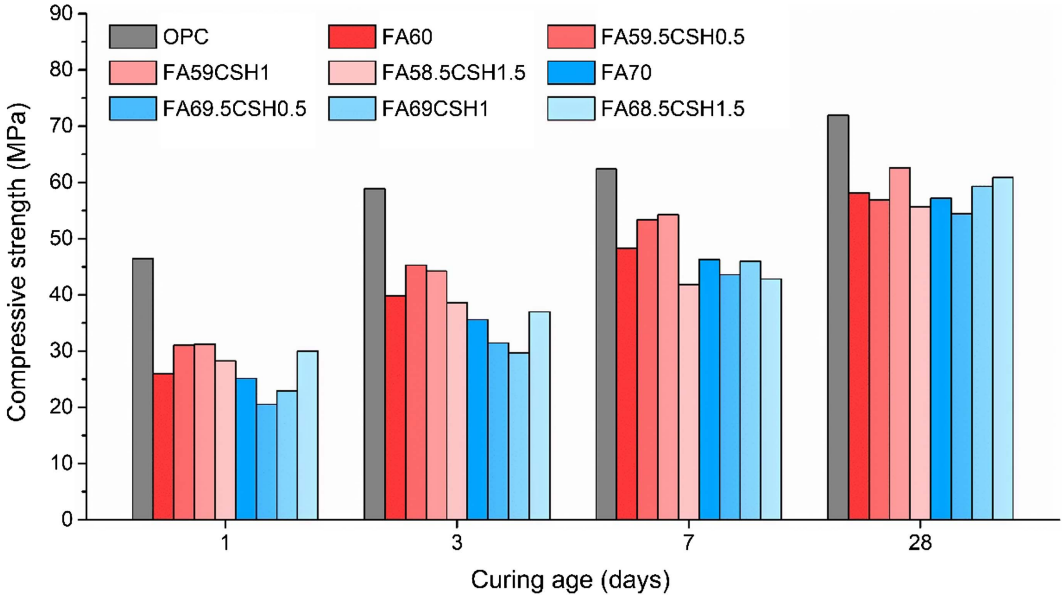

Fig. 3. Compressive strength development of concrete mixes.

J. Mater. Civ. Eng., 2021, 33(12): 04021356

Table 3. Elemental composition of pastes obtained from XRF

Formula	Z	Concentration				
		OPC (%)	FA60 (%)	FA70 (%)	FA59CSH1 (%)	FA68.5CSH1.5 (%)
Al_2O_3	13	3.73	12.33	12.77	11.89	12.57
SiO_2	14	16.81	25.41	26.31	25.32	25.41
CaO	20	70.63	48.06	45.95	48.46	46.83
Fe_2O_3	26	3.37	8.41	9.00	8.48	9.26

X-Ray Fluorescence

Table 3 shows the XRF data for selected samples at 28 days. Z stands for the atomic number of an element. Observe that the chemical compositions of HVFA samples were significantly different from those of OPC. The SiO_2 content in OPC was 16.81%, and it was more than 25% in HVFA samples. The Al_2O_3 content in OPC was only 3.73%, but it was greater than 10% in HVFA concrete. This finding was attributed to the fact that SiO_2 and Al_2O_3 are the major components of fly ash. Moreover, OPC samples contained fewer Fe_2O_3 and more CaO contents than HVFA concrete due to the difference in the major components of OPC and fly ash. However, the differences among HVFA mixes with and without nano-CHS crystals were insignificant. The contents of Al_2O_3 and SiO_2 in FA59CSH1 and FA68.5CSH1.5 were slightly smaller than those in FA60 and FA70 due to the replacement of fly ash with nano-CSH crystals.

Thermogravimetric Analysis

The TG and DTG curves for all of the pastes are in Figs. 4–8. The curves for all of the pastes demonstrated reasonable trends that the loss of weight increases with the increase of age, as the hydration product increases over time. Three major sags could be seen in each DTG curve corresponding to the mass loss due to Ldh, Ldx, and Ldc.

From Table 4, where Ldh, Ldx, and Ldc values of the mixes are presented, note that FA59CSH1 and FA68.5CSH1.5 have higher Ldh values compared with FA60 and FA70, respectively. Ldh is the chemically bound water from C-S-H. It indicates that adding nano-CSH crystals facilitates the formation of C-S-H in the HVFA pastes. This result agrees well with the compressive strength results that higher strength could be seen in the HVFA mixes with nano-CSH crystals. Comparing Ldc as the chemically bond water from $CaCO_3$ among different mixes, the pure HVFA mixes have higher

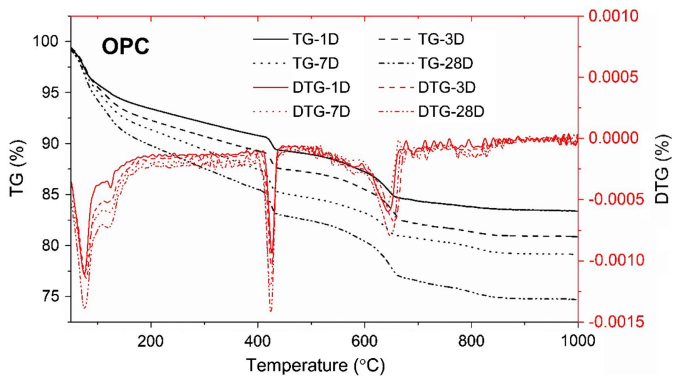

Fig. 4. TG and DTG curves for OPC paste at the ages of 1, 3, 7, and 28 days.

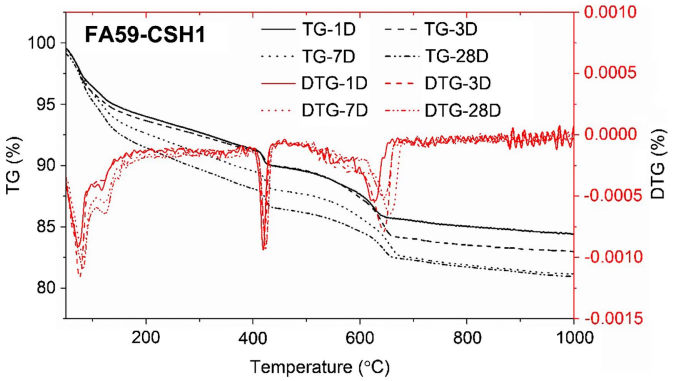

Fig. 6. TG and DTG curves for FA59CSH1 paste at the ages of 1, 3, 7, and 28 days.

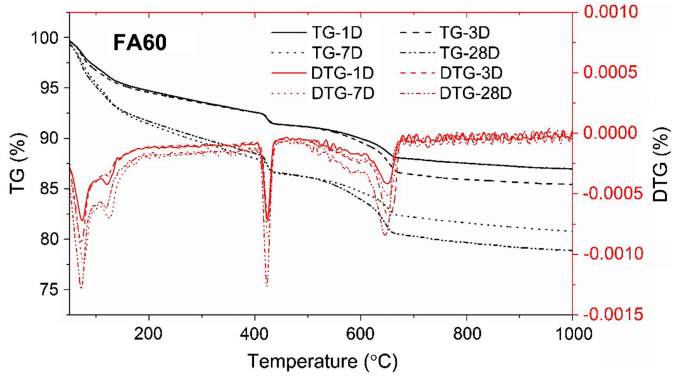

Fig. 5. TG and DTG curves for FA60 paste at the ages of 1, 3, 7, and 28 days.

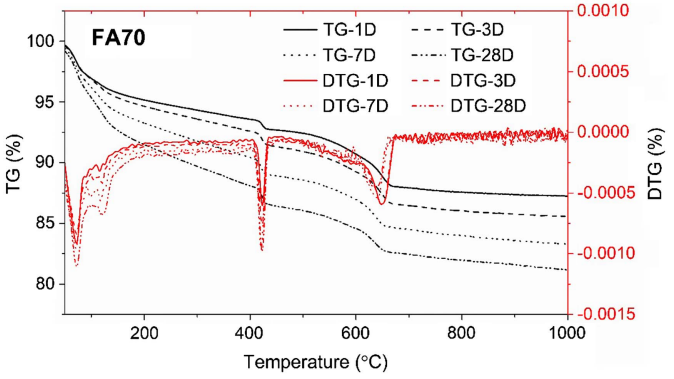

Fig. 7. TG and DTG curves for FA70 paste at the ages of 1, 3, 7, and 28 days.

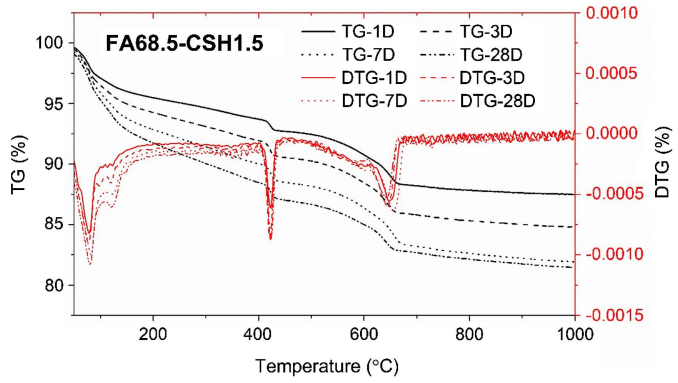

Fig. 8. TG and DTG curves for FA68.5CSH1.5 paste at the ages of 1, 3, 7, and 28 days.

Table 4. Ldh, Ldx, and Ldc of the mixes

Mixes	Ldh	Ldx	Ldc
OPC	8.38	5.11	5.69
FA60	5.23	4.57	5.075
FA70	5.74	3.50	3.41
FA59CSH1	7.24	3.50	3.68
FA68.5CSH1.5	6.56	3.48	3.56

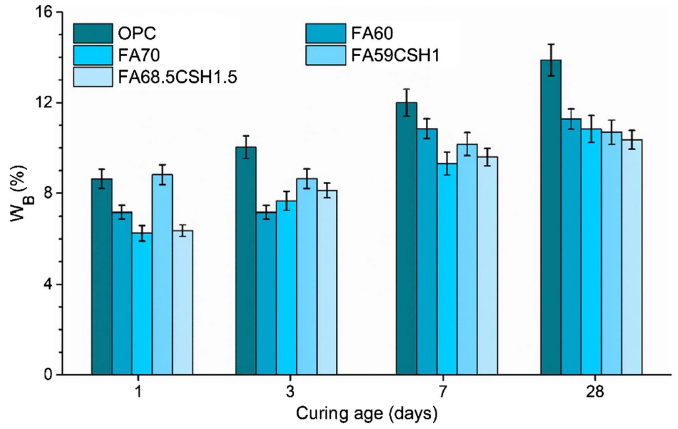

Fig. 9. Chemically bound water (W_B) for paste OPC, FA60, FA70, FA59CSH1, and FA58.5CSH1.5.

Ldc values compared with the mixes with nano-CSH crystals. The $CaCO_3$ content is from the carbonation of $Ca(OH)_2$ during hydration. This could reflect that the pure HVFA mixes without nano-CSH crystals are more prone to carbonation. The Ldx value represents the decomposition of $Ca(OH)_2$ in the mixes. However, the actual amount of $Ca(OH)_2$ in the mixes are composed of the weight both from Ldx [decomposition of $Ca(OH)_2$] and Ldc (decomposition of $CaCO_3$), as $Ca(OH)_2$ carbonate to form $CaCO_3$. The actual $Ca(OH)_2$ content for the mixes are calculated and presented in Fig. 10.

Chemically bound water and $Ca(OH)_2$ content values are calculated from the Ldh, Ldx, and Ldc of the mixes. Fig. 9 shows the chemically bound water in the pastes. Among all pastes without nano-CSH crystals, OPC shows the highest W_B, and FA70 demonstrates lowest W_B at all of the ages of 1, 3, 7, and 28 days. Therefore, increasing the content of FA decreased the hydration products

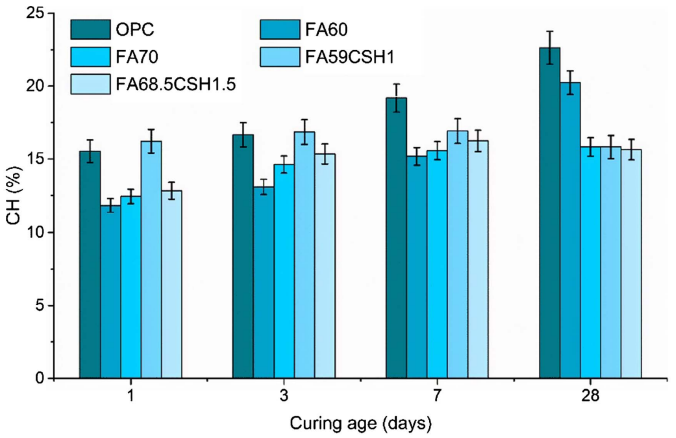

Fig. 10. Actual $Ca(OH)_2$ (CH) content for paste OPC, FA60, FA70, FA59CSH1, and FA58.5CSH1.5.

in the pastes. This could be explained by the postponed hydration of FA compared with OPC (Lothenbach et al. 2011; Neville 2011).

After the addition of 1% nano-CSH seeds, FA59CSH1 had a higher content of chemically bound water than FA60 at 1, 3, 7, and 28 days. Similarly, FA68.5CSH1.5 contained more chemically bound water than FA70. Adding nano-CSH seeds could stimulate the hydration of HVFA pastes containing 60% and 70% fly ash. Furthermore, the effect of nano-CSH seeds on FA60 was more significant than it was on FA70, in particular when the age was less than 3 days.

Fig. 10 shows the $Ca(OH)_2$ content in OPC, FA60, FA70, FA59CSH1, and FA68.5CSH1.5 pastes. Note that the $Ca(OH)_2$ content decreased with the increase of fly ash dosage in cement pastes at 1, 3, 7, and 28 days when comparisons were made among OPC, FA60, and FA70 pastes. With less portland cement in FA60 and FA70 pastes, less $Ca(OH)_2$ could be generated from hydration. After adding nano-CSH crystals, FA59CSH1 and FA68.5CSH1.5 had higher $Ca(OH)_2$ content than FA60 and FA70 pastes at the ages of 1, 3, and 7 days, respectively. However, the $Ca(OH)_2$ content of FA59CSH1 and FA68.5CSH1.5 pastes on the 28th day became lower than those of FA60 and FA70, respectively. It is known that the hydration of OPC generates $Ca(OH)_2$, whereas the hydration of fly ash consumes $Ca(OH)_2$.

The variation of $Ca(OH)_2$ in the pastes indicated that the formation of $Ca(OH)_2$ from OPC hydration exceeded the consumption of $Ca(OH)_2$ by the hydration of fly ash in FA59CSH1 and FA68.5CSH1.5 pastes at the early ages of 1, 3, and 7 days. On the 28th day, the $Ca(OH)_2$ consumed by fly ash hydration in FA59CSH1 and FA68.5CSH1.5 finally exceeded the $Ca(OH)_2$ generated from OPC hydration. Adding nano-CSH crystals facilitated the consumption of FA in HVFA mixes, or the pozzolanic reaction between FA and $Ca(OH)_2$ to form C-S-H. Improved pozzolanic reaction of FA concrete by the addition of other nanoparticles, mostly nano-silica and nano-$CaCO_3$, can be found in the previous literature (Said and Zeidan 2009; Supit and Shaikh 2014; Liu et al. 2020).

Fourier-Transform Infrared Spectroscopy

Fig. 11 shows the FTIR results for all samples at the ages of 1, 3, 7, and 28 days. The broad bands present in the range of 3,648 –3,650 cm^{-1} of all of the samples is associated with the overlapping stretching vibration of the −OH groups of $Ca(OH)_2$ from the tricalcium silicates (C_3S) and dicalcium silicates (C_2S) hydration

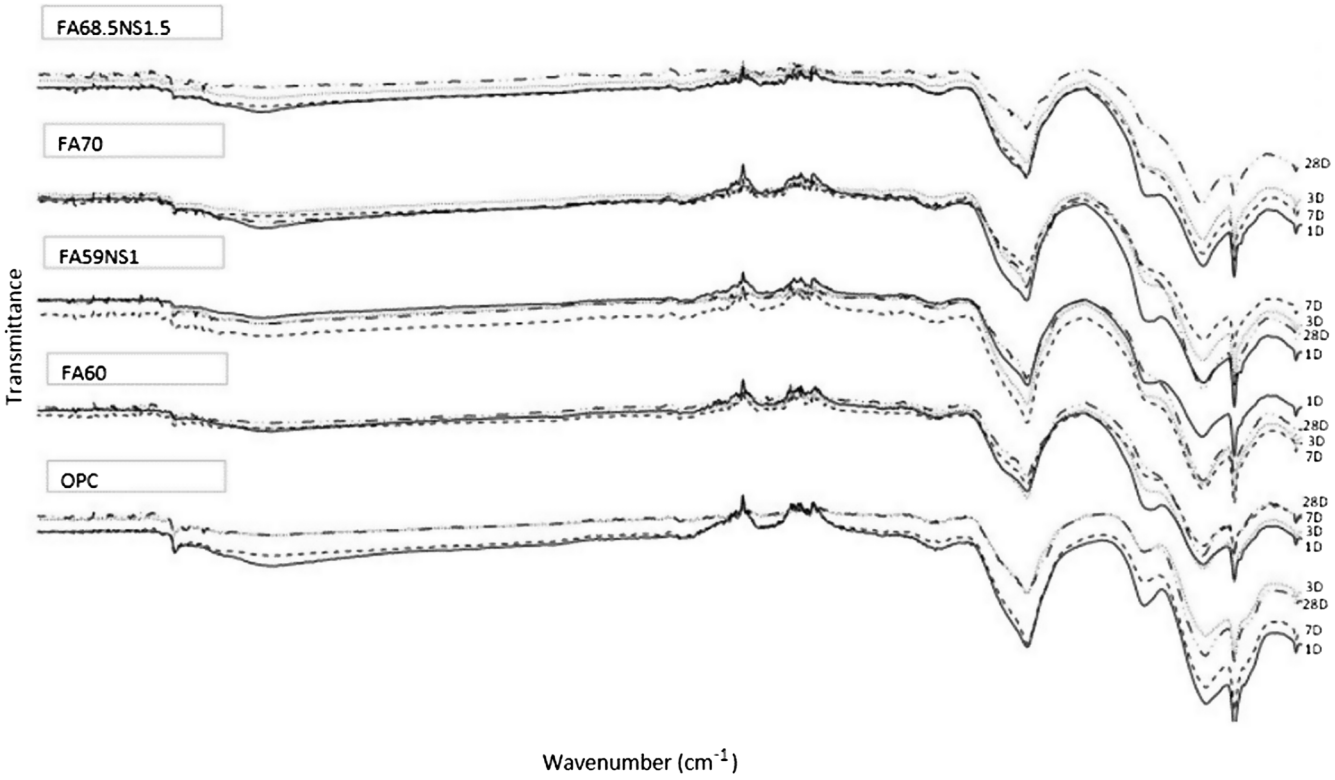

Fig. 11. FTIR for OPC and HVFA pastes.

and the free −OH groups of water molecules in the mixes (Biricika and Sarierb 2014). Note that the band diminished with the increase of hydration time from 1 to 28 days, indicating the decrease of free water as a result of CSH formation. Comparisons among the −OH groups of different mixes suggest that OPC showed the largest decrease of this band from 1 to 28 days, but FA60 and FA70 had the least significant decrease. The hydration of OPC generated more CSH than HVFA mixes because the reaction of fly ash is slower than OPC, especially at an early age (Bremseth 2009; Neville 2011). Compared to HVFA pastes FA60 and FA70, FA59CSH1 and FA68.5CSH1.5 had a more remarkable decrease in the intensity of the −OH groups between 1 and 28 days. The decrease of −OH groups in HVFA pastes with nano-CSH crystals could be induced by either the consumption by fly ash or less free water present, which has been demonstrated by TGA results. The TGA results show that adding nano-CSH crystals increased the content of CSH, so less free water was available. Note that less $Ca(OH)_2$ could be found in the HVFA pastes with nano-CSH crystals compared with pure HVFA pastes.

The bands between 949 and 719 cm^{-1} correspond to the bending-in-plane vibrations of the Si–O bonds in C_3S and C_2S. The intensity of the bands decreased with the formation of CSH over time. For HVFA pastes with nano-CSH crystals, the peak intensity of Si–O bonds decreased more substantially than HVFA paste, indicating that adding nano-CSH crystals increased the content of CSH after the hydration of the pastes.

The bands in the wave number range of 1410–1510 cm^{-1} are associated with the C–O functional group due to the carbonation by the reaction between $Ca(OH)_2$ and CO_2 in the air (Chang and Chen 2006; Biricika and Sarierb 2014). At 28 days, the peak intensity of FA59CSH1 and FA68.5CSH1.5 was smaller compared with FA60 and FA70. This result matches with the TGA findings. It indicates that the HVFA mixes with nano-CSH crystals has a lesser degree of carbonation compared with pure HVFA mixes.

Scanning Electron Microscopy

Fig. 12 shows the SEM images of OPC and HVFA pastes. Observe from the images with a magnification of 2,000× that round fly ash particles could be seen in HVFA pastes but not in OPC. Compared with FA60 and FA70, fewer fly ash particles were observed in FA59CSH1 and FA68.5CSH1.5 because fly ash was consumed by adding nano-CSH crystals. This observation agrees well with the TGA results. Existing research (Lau 2011) demonstrates denser hydration product if incorporating nano-CSH crystals in OPC mix. Besides being effective in OPC mix as previously mentioned (Lau 2011), adding nano-CSH crystals in HVFA mixes could densify the hydration product, as well. In the images with a magnification of 10,000× times, where C-S-H could be observed more clearly, the hydration product that formed surrounding the nano-CSH crystals for FA59CSH1 and FA68.5CSH1.5 mixes were denser compared with pure HVFA pastes. This result could be closely associated with the results revealed in the previous sections, showing improved compressive strength and carbonation resistance of HVFA pastes with nano-CSH crystals.

Conclusion

This research investigated the microstructure of the high-volume fly ash (HVFA) composites with the addition of nano-CSH crystals to understand the effectiveness of nano-CSH crystals in enhancing the early-age strength development of HVFA concrete. The findings are summarized as follows:

1. Addition of 1% and 1.5% nano-CSH crystals could increase the early-age compressive strength of HVFA concrete with 60% and 70% fly ash replacement ratio, respectively.
2. With the addition of nano-CSH crystals to HVFA pastes, the TGA, FTIR, and SEM tests reveal that more fly ash was consumed to generate C-S-H in the hydration process; therefore,

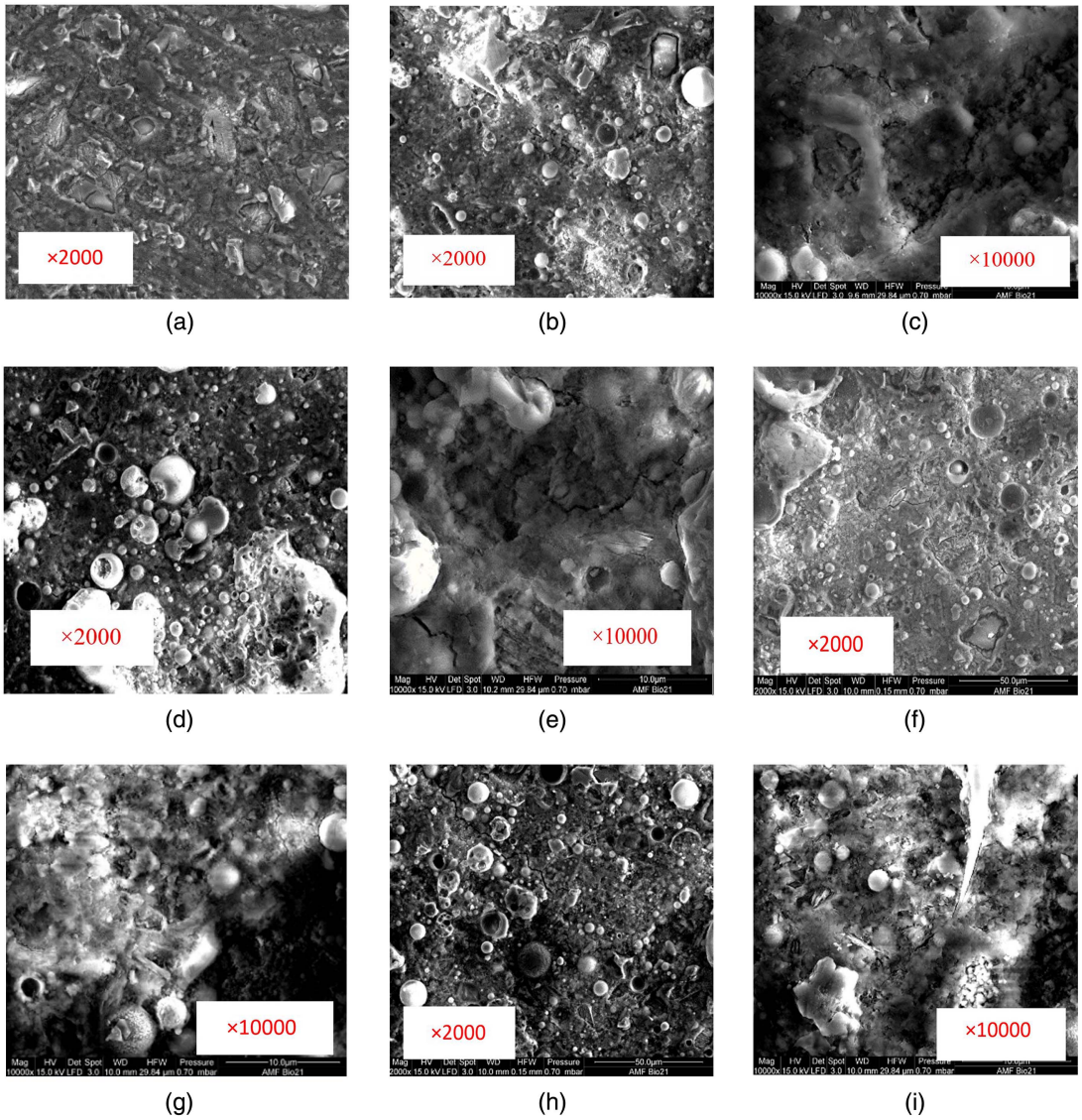

Fig. 12. SEM images for the OPC and HVFA pastes: (a) OPC; (b) FA60x2,000; (c) FA60x10,000; (d) FA70x2,000; (e) FA70x10,000; (f) FA59CSH1x2,000; (g) FA59CSH1x10,000; (h) FA68.5CSH1.5x2,000; and (i) FA68.5CSH1.5x10,000.

less $Ca(OH)_2$ was left in the hydration product. This improved pozzolanic reaction results in the increased compressive strength of HVFA pastes with the addition of nano-CSH crystals.

3. The TGA and FTIR tests show that adding 1% and 1.5% nano-CSH crystal to HVFA pastes reduced the $CaCO_3$ content of HVFA with 60% and 70% fly ash replacement ratios. This could be due to the denser microstructure of HVFA pastes with the addition of nano-CSH crystals compared with pure HVFA pastes, indicated by SEM images.

Data Availability Statement

All data, models, and code generated or used during the study appear in the published article.

Acknowledgments

All of the authors would like to acknowledge the financial support from the Melbourne Research Scholarship offered by the University of Melbourne and the Australian Research Council's Discovery Early Career Researcher Grant (Nos. DE170100165 and DE 2017 R1). We would like to thank Cement Australia and BASF Australia for offering the material and concrete admixture for experimental programs. We also would like to express our gratitude for Laura Jukes's help with part of the experimental preparation.

References

Ahmad Fara, A. N. K., and H. Z. Abdullah. 2016. "Influence of calcination temperature on the microstructure and crystallographic properties of hydroxyapatite from black Tilapia fish scale." In Vol. 840 of *Materials science forum*, 151–155. Freienbach, Switzerland: Trans Tech Publications Ltd. https://doi.org/10.4028/www.scientific.net/MSF.840.151.

Alaka, H. A., L. O. Oyedele, and O. L. Toriola-Coker. 2016. "Effect of excess dosages of superplasticizer on the properties of highly sustainable high-volume fly ash concrete." *Int. J. Sustainable Build. Technol. Urban Dev.* 7 (2): 73–86. https://doi.org/10.1080/2093761X.2016.1167643.

ASTM. 2005. *Standard specification for coal fly ash and raw or calcined natural pozzolan for use in concrete*. ASTM C618-05. West Conshohocken, PA: ASTM.

BASF (Badische Anilin-und-Soda-Fabrik). 2015. *Master X-Seed 1500. BASF Safety data sheet*. Southbank, VIC, Australia: BASF.
BASF (Badische Anilin-und-Soda-Fabrik). 2020a. *MasterGlenium® ACE 8710*. Southbank, VIC, Australia: BASF.
BASF (Badische Anilin-und-Soda-Fabrik). 2020b. *MasterXSeed1500*. Southbank, VIC, Australia: BASF.
Bhatty, J. 1986. "Hydration versus strength in a portland cement developed from domestic mineral wastes—A comparative study." *Thermochim. Acta* 106 (1986): 93–103. https://doi.org/10.1016/0040-6031(86)85120-6.
Biricika, H., and N. Sarierb. 2014. "Comparative study of the characteristics of nano Silica-, Silica fume- and fly ash-incorporated cement mortars." *Mater. Res.* 17 (3): 570–582. https://doi.org/10.1590/S1516-14392014005000054.
Bremseth, S. K. 2009. *Fly ash in concrete—A literature review of the advantages and disadvantages*. Oslo, Norway: SINTEF Building and Infrastructure.
Chang, C.-F., and J.-W. Chen. 2006. "The experimental investigation of concrete carbonation depth." *Cem. Concr. Res.* 36 (9): 1760–1767. https://doi.org/10.1016/j.cemconres.2004.07.025.
Deboucha, W., N. Leklou, A. Khelidj, and M. N. Oudjit. 2017. "Hydration development of mineral additives blended cement using thermogravimetric analysis (TGA): Methodology of calculating the degree of hydration." *Constr. Build. Mater.* 146 (2017): 687–701. https://doi.org/10.1016/j.conbuildmat.2017.04.132.
Gong, J., Z. P. Li, R. T. Zhang, J. F. Li, and X. M. Shi. 2019. "Synergistic effects of nano-montmorillonite and polyethylene microfiber in foamed paste with high volume fly ash binder." *J. Nanosci. Nanotechnol.* 19 (8): 4465–4473. https://doi.org/10.1166/jnn.2019.16353.
Hemalatha, T., and S. Sasmal. 2019. "Early-age strength development in fly ash blended cement composites: Investigation through chemical activation." *Mag. Concr. Res.* 71 (5): 260–270. https://doi.org/10.1680/jmacr.17.00336.
Huang, C. H., S. K. Lin, C. S. Chang, and H. J. Chen. 2013. "Mix proportions and mechanical properties of concrete containing very high-volume of Class F fly ash." *Constr. Build. Mater.* 46 (Sep): 71–78. https://doi.org/10.1016/j.conbuildmat.2013.04.016.
Jalal, M., A. Pouladkhan, O. F. Harandi, and D. Jafari. 2015. "Comparative study on effects of Class F fly ash, nano silica and silica fume on properties of high performance self compacting concrete." *Constr. Build. Mater.* 94 (Sep): 90–104. https://doi.org/10.1016/j.conbuildmat.2015.07.001.
Kawashima, S., P. K. Hou, D. J. Corr, and S. P. Shah. 2013. "Modification of cement-based materials with nanoparticles." *Cem. Concr. Compos.* 36 (Feb): 8–15. https://doi.org/10.1016/j.cemconcomp.2012.06.012.
Kawashima, S., J. W. T. Seo, D. Corr, M. C. Hersam, and S. P. Shah. 2014. "Dispersion of $CaCO_3$ nanoparticles by sonication and surfactant treatment for application in fly ash–cement systems." *Mater. Struct.* 47 (6): 1011–1023. https://doi.org/10.1617/s11527-013-0110-9.
Klimesch, D. S., and A. Ray. 1996. "The use of DTA/TGA to study the effects of ground quartz with different surface areas in autoclaved cement: Quartz pastes. Part 1: A method for evaluating DTA/TGA results." *Thermochim. Acta* 289 (1): 41–54. https://doi.org/10.1016/S0040-6031(96)03033-X.
Kocak, Y., and S. Nas. 2014. "The effect of using fly ash on the strength and hydration characteristics of blended cements." *Constr. Build. Mater.* 73 (Dec): 25–32. https://doi.org/10.1016/j.conbuildmat.2014.09.048.
Lau, B. 2011. "From nanocrystals to concrete components: X-SEED® crystals from BASF make concrete harden faster and reduce carbon emissions." Accessed June 6, 2021. https://www.basf.com/us/en/media/science-around-us/from-nanocrystals-to-concrete-components.html.
Liu, H., Y. Zhang, R. Tong, Z. Zhu, and Y. Lv. 2020. "Effect of nano-silica on impermeability of cement-fly ash system." *Adv. Civ. Eng.* 2020: 1243074. https://doi.org/10.1155/2020/1243074.
Liu, M., H. B. Tan, and X. Y. He. 2019. "Effects of nano-SiO_2 on early strength and microstructure of steam-cured high volume fly ash cement system." *Constr. Build. Mater.* 194 (Jan): 350–359. https://doi.org/10.1016/j.conbuildmat.2018.10.214.
Lothenbach, B., K. Scrivener, and R. D. Hooton. 2011. "Supplementary cementitious materials." *Cem. Concr. Res.* 41 (12): 1244–1256. https://doi.org/10.1016/j.cemconres.2010.12.001.
Ma, B. G., H. N. Li, X. G. Li, J. P. Mei, and Y. Lv. 2016. "Influence of nano-TiO_2 on physical and hydration characteristics of fly ash–cement systems." *Constr. Build. Mater.* 122 (Sep): 242–253. https://doi.org/10.1016/j.conbuildmat.2016.02.087.
Malhotra, V. M., and P. K. Mehta. 2002. *High-performance, high-volume fly ash concrete: Materials, mixture proportioning, properties, construction practice, and case histories*. Oak Ridge, TN: US Dept. of Energy Office of Scientific and Technical Information.
Mohseni, E., B. M. Miyandehi, J. Yang, and M. A. Yazdi. 2015. "Single and combined effects of nano-SiO_2, nano-Al_2O_3 and nano-TiO_2 on the mechanical, rheological and durability properties of self-compacting mortar containing fly ash." *Constr. Build. Mater.* 84 (Jun): 331–340. https://doi.org/10.1016/j.conbuildmat.2015.03.006.
Nazari, A., and S. Riahi. 2011. "The effects of zinc dioxide nanoparticles on flexural strength of self-compacting concrete." *Composites, Part B* 42 (2): 167–175. https://doi.org/10.1016/j.compositesb.2010.09.001.
Neville, A. M. 2011. *Properties of concrete* Essex, England: Pearson Education.
Niewiadomski, P., D. Stefaniuk, and J. Hola. 2017. "Microstructural analysis of self-compacting concrete modified with the addition of nano-particles." *Modern Build. Mater. Struct. Techn.* 172: 776–783.
Nonat, A. 2010. "C-S-H and concrete properties." *Cem. Wapno, Beton* 15 (6): 315–326.
Oltulu, M., and R. Şahin. 2013. "Effect of nano-SiO_2, nano-Al_2O_3 and nano-Fe_2O_3 powders on compressive strengths and capillary water absorption of cement mortar containing fly ash: A comparative study." *Energy Build.* 58 (Mar): 292–301. https://doi.org/10.1016/j.enbuild.2012.12.014.
PerkinElmer. 2005. "Spectrum 100 series user's guide." Accessed October 6, 2020. https://www.usf.edu/research-innovation/rf/usf-connect/documents/perkin-elmer-spectrum-100-ftir-users-guide.pdf.
Said, A. M., and M. S. Zeidan. 2009. "Enhancing the reactivity of normal and fly ash concrete using colloidal nano-silica." *Spec. Publ.* 267: 75–86.
Shaikh, F. U. A., and S. W. M. Supit. 2014. "Mechanical and durability properties of high volume fly ash (HVFA) concrete containing calcium carbonate ($CaCO_3$) nanoparticles." *Constr. Build. Mater.* 70 (Nov): 309–321. https://doi.org/10.1016/j.conbuildmat.2014.07.099.
Shaikh, F. U. A., and S. W. M. Supit. 2015. "Chloride induced corrosion durability of high volume fly ash concretes containing nano particles." *Constr. Build. Mater.* 99 (Nov): 208–225. https://doi.org/10.1016/j.conbuildmat.2015.09.030.
Shaikh, F. U. A., S. W. M. Supit, and S. Barbhuiya. 2017. "Microstructure and nanoscaled characterization of HVFA cement paste containing nano-SiO_2 and nano-$CaCO_3$." *J. Mater. Civ. Eng.* 29 (8): 04017063. https://doi.org/10.1061/(ASCE)MT.1943-5533.0001898.
Shaikh, F. U. A., S. W. M. Supit, and P. K. Sarker. 2014. "A study on the effect of nano silica on compressive strength of high volume fly ash mortars and concretes." *Mater. Des.* 60 (Aug): 433–442. https://doi.org/10.1016/j.matdes.2014.04.025.
Siddique, R. 2004. "Performance characteristics of high-volume Class F fly ash concrete." *Cem. Concr. Res.* 34 (3): 487–493. https://doi.org/10.1016/j.cemconres.2003.09.002.
Sofi, M., P. A. Mendis, and D. Baweja. 2012. "Estimating early-age in situ strength development of concrete slabs." *Constr. Build. Mater.* 29 (Apr): 659–666. https://doi.org/10.1016/j.conbuildmat.2011.10.019.
Sofi, M., P. A. Mendis, S. Lie, and D. Baweja. 2008. "Early age concrete thermal and creep effects: Relevance to anchorage zones of post-tensioned members." *Electron. J. Struct. Eng.* 8: 90–96.
Soutsos, M., A. Hatzitheodorou, J. Kwasny, and F. Kanavaris. 2016. "Effect of in situ temperature on the early age strength development of concretes with supplementary cementitious materials." *Constr. Build. Mater.* 103 (Jan): 105–116. https://doi.org/10.1016/j.conbuildmat.2015.11.034.
Sun, J. F., X. D. Shen, G. Tan, and J. E. Tanner. 2019. "Modification effects of nano-SiO_2 on early compressive strength and hydration

characteristics of high-volume fly ash concrete." *J. Mater. Civ. Eng.* 31 (6): 04019057. https://doi.org/10.1061/(ASCE)MT.1943-5533.0002665.
Supit, S. W. M., and F. U. A. Shaikh. 2015. "Durability properties of high volume fly ash concrete containing nano-silica." *Mater. Struct.* 48 (8): 2431–2445. https://doi.org/10.1617/s11527-014-0329-0.
Szostak, B., and G. L. Golewski. 2018. "Effect of nano admixture of CSH on selected strength parameters of concrete including fly ash." In Vol. 416 of *Proc., IOP Conf. Series: Materials Science and Engineering*, 012105. Bristol, UK: IOP Publishing.
Thomas, M. 2007. *Optimizing the use of fly ash concrete*. Skokie, IL: Portland Cement Association.
Tomczyk, A., Z. Sokołowska, and P. Boguta. 2020. "Biochar physicochemical properties: Pyrolysis temperature and feedstock kind effects." *Rev. Environ. Sci. Biotechnol.* 19 (1): 191–215. https://doi.org/10.1007/s11157-020-09523-3.
Wang, L., H. L. Zhang, and Y. Gao. 2018. "Effect of TiO_2 Nano-particles on physical and mechanical properties of cement at low temperatures." In *Advances in materials science and engineering*. London: Hindawi.
Wongkeo, W., P. Thongsanitgarn, A. Ngamjarurojana, and A. Chaipanich. 2014. "Compressive strength and chloride resistance of self-compacting concrete containing high level fly ash and silica fume." *Mater. Des.* 64 (Dec): 261–269. https://doi.org/10.1016/j.matdes.2014.07.042.
Xiao, L., and B. Pang. 2017. "Experimental study on the effect of calcination on the volcanic ash activity of diatomite." In *Proc., IOP Conf. Series: Materials Science and Engineering*, 012089. Bristol, UK: IOP Publishing.
Yang, J., E. Mohseni, B. Behforouz, and M. M. Khotbehsara. 2015. "An experimental investigation into the effects of Cr_2O_3 and ZnO_2 nanoparticles on the mechanical properties and durability of self-compacting mortar." *Int. J. Mater. Res.* 106 (8): 886–892. https://doi.org/10.3139/146.111245.
Zhang, M. H., and J. Islam. 2012. "Use of nano-silica to reduce setting time and increase early strength of concretes with high volumes of fly ash or slag." *Constr. Build. Mater.* 29 (Apr): 573–580. https://doi.org/10.1016/j.conbuildmat.2011.11.013.
Zhang, M. H., J. Islam, and S. Peethamparan. 2012. "Use of nano-silica to increase early strength and reduce setting time of concretes with high volumes of slag." *Cem. Concr. Compos.* 34 (5): 650–662. https://doi.org/10.1016/j.cemconcomp.2012.02.005.
Zhang, R., X. Cheng, P. K. Hou, and Z. M. Ye. 2015. "Influences of nano-TiO_2 on the properties of cement-based materials: Hydration and drying shrinkage." *Constr. Build. Mater.* 81 (Apr): 35–41. https://doi.org/10.1016/j.conbuildmat.2015.02.003.
Zhu, J. P., C. H. Feng, H. B. Yin, Z. Y. Zhang, and S. P. Shah. 2015. "Effects of colloidal nanoBoehmite and nanoSiO_2 on fly ash cement hydration." *Constr. Build. Mater.* 101: 246–251. https://doi.org/10.1016/j.conbuildmat.2015.10.038.